Spike Sequence Learning in a Photonic Spiking Neural Network Consisting of VCSELs-SA With Supervised Training

Ziwei Song, Shuiying Xiang, Zhenxing Ren, Genquan Han, and Yue Hao

***Abstract*—We propose a fully-connected photonic spiking neural network (SNN) consisting of excitable vertical-cavity surface-emitting lasers with an embedded saturable absorber (VCSELs-SA) to implement spike sequence learning by a supervised training. The photonic spike-timing-dependent plasticity (STDP) is incorporated into a classical remote supervised method (ReSuMe) algorithm to implement supervised training of a photonic SNN for the first time. The computation model of the photonic SNN is derived based on the Yamada model. To optimize the learning process, we further propose a novel measure, the so-called spike sequence distance, to quantitatively evaluate the effects of controllable parameters. The numerical results show that, the photonic SNN successfully reproduces a desirable output spike sequence in response to a spatiotemporal input spike pattern by means of the iteration algorithm to update synaptic weights continuously. These results contribute one step forward toward the device-algorithm co-design and optimization of the all-VCSELs-based energy-efficient photonic SNN.**

***Index Terms*—Photonic spiking neural network, vertical-cavity surface-emitting lasers, photonic spike-timing-dependent plasticity, supervised spike sequence learning.**

I. Introduction

THE human brain with superior information processing capabilities and advanced learning mechanisms can perform complicated tasks with ultralow power consumption [1]. These excellent performances originate from a high parallelism of information storage and processing in the brain. The conventional artificial intelligence based on the von Neumann architecture has hit the limitations of energy and speed due to the separated memory and processing units [2]. Inspired by the human brain, neuromorphic computing which is a promising breakthrough beyond the von Neumann computing has attracted considerable attention.

The approach for the efficient implementation of the neuromorphic computing is to construct artificial neural networks (ANNs) which mimic the structure and operation of the human brain [3]. Different from the traditional ANNs, the unique feature of the human brain is the event-driven scheme of computation which is the representation of information via binary spikes [4]. Consequently, spiking neural networks (SNNs), which are usually called the third generation of neural networks, are introduced to emulate the style of information processing in the human brain [5]. Hence, SNNs are more biologically plausible and computationally efficient than the conventional ANNs [6], [7].

A SNN for neuromorphic computing contains artificial neurons, artificial synapses and learning algorithms [8]. Learning and memory processes in a neural network can be performed simultaneously by adjusting the connection strength of synapses linking two adjacent neurons with the help of appropriate learning algorithms. To date, tremendous efforts have been made to develop neuromorphic devices and systems with an ultimate goal of the implementation of brain-like neuromorphic computing. Specifically, an enormous variety of technologies in the electronic fields have been employed to develop neuromorphic devices and circuits including the complementary metal oxide semiconductor (CMOS) [9]–[11], transistors [12]–[14] and the emerging non-volatile memory technologies [15]–[18]. These brain-inspired neuromorphic electronic approaches break the bottleneck of the von Neumann architecture, but still suffer from the limitations of energy-efficiency and operation speed due to the bandwidth-connection-density trade-off [19].

Photonic technology is a promising alternative for the implementation of ultra-fast neural computing and information processing with much lower power consumption and faster speed compared to the electronic counterparts. Neuromorphic computing based on photonic technology becomes an emerging filed. Photonic spiking neurons and synapses are two basic functional elements in the neuromorphic photonic SNNs. In recent years, various photonic neurons [20]–[39], photonic synapses

Manuscript received December 1, 2019; revised February 12, 2020 and February 13, 2020; accepted February 14, 2020. Date of publication February 28, 2020; date of current version March 9, 2020. This work was supported in part by the National Natural Science Foundation of China under Grants 61974177 and 61674119, in part by the Postdoctoral innovation talent program in China under Grant BX201600118, in part by the project funded by China Postdoctoral Science Foundation under Grant 2017M613072, and in part by Postdoctoral Science Foundation in Shaanxi Province of China. *(Corresponding author: Shuiying Xiang.)*

Ziwei Song and Zhenxing Ren are with the State Key Laboratory of Integrated Service Networks, Xidian University, Xi'an 710071, China (e-mail: 1064971297@qq.com; 584401206@qq.com).

Shuiying Xiang is with the State Key Laboratory of Integrated Service Networks, Xidian University, Xi'an 710071, China, and also with the State Key Discipline Laboratory of Wide Bandgap Semiconductor Technology, School of Microelectronics, Xidian University, Xi'an 710071, China (e-mail: syxiang@xidian.edu.cn).

Genquan Han and Yue Hao are with the State Key Discipline Laboratory of Wide Bandgap Semiconductor Technology, School of Microelectronics, Xidian University, Xi'an 710071, China (e-mail: gqhan@xidian.edu.cn; yhao@xidian.edu.cn).

Color versions of one or more of the figures in this article are available online at http://ieeexplore.ieee.org.

Digital Object Identifier 10.1109/JSTQE.2020.2975564

[40]–[47], and photonic neural networks [24], [26]–[28], [37], [48] have gained great progress. For instance, Hurtado and Deng *et al.* demonstrated that vertical-cavity surface-emitting lasers (VCSELs) exhibited certain neuron-like dynamics and could be served as photonic neurons [20], [22], [30]–[32]. Furthermore, a VCSEL with an embedded saturable absorber (VCSEL-SA) exhibits excitability and behaves analogously to a leaky integrate-and-fire (LIF) neuron [24], [34]–[38]. Hence, the VCSEL-SA is an ideal photonic spiking neuron device for a photonic SNN. Note that, the major advantage of VCSELs is easy integration. Hence, the advancement in the photonic integration technology enables building a large network with up to several hundreds of VCSELs-SA experimentally [49]. On the other hand, the VCSEL operating below threshold can serve as a vertical-cavity semiconductor optical amplifier (VCSOA), and enables the implementation of photonic spike-timing-dependent plasticity (STDP) with lower power consumption [47]. Furthermore, the STDP-based unsupervised spiking learning in a photonic SNN composed of VCSELs-SA was numerically realized in our previous work [48]. Note, there is a biological evidence that the brain performs certain cognitive tasks via supervised or instruction-based learning [50], [51]. Supervised learning is an important biomimetic concept of information processing in the neural network, which means that a network is trained to output desired results by the instruction of a teacher neuron. Hence, it is of great significance to develop suitable and effective supervised learning algorithms to exploit the powerful computing capability and broad application prospects of SNNs.

However, a photonic SNN based on neuromorphic devices with brain-like supervised learning algorithms still remains a significant challenge. In this paper, we propose a two-layer fully-connected photonic SNN based on excitable VCSELs-SA to implement spike sequence learning by a supervised training manner. As a representative task of supervised learning, spike sequence learning enables a neural network to learn and precisely reproduce arbitrary desired target spike sequences. To the best of our knowledge, this is the first time that the supervised multi-target recognition is realized in a photonic SNN. Specifically, we incorporate the photonic STDP into a classical supervised learning algorithm, i.e., the remote supervised method (ReSuMe), to train the proposed photonic SNN [52].

The rest of this paper is organized as follows. In Section II, the photonic SNN architecture for spike sequence learning is introduced. The theoretical model of photonic spiking neurons based on VCSELs-SA is also described. Besides, the principle of the ReSuMe algorithm combining the photonic STDP is explained. Additionally, we also define the spike sequence distance to measure the similarity of a pair of spike sequences. In Section III, we elaborate the learning process of the spike sequence with the photonic SNN. Then, the optimization of the supervised learning algorithm is analyzed. The effects of the initial weights and the number of pre-synaptic neurons on the supervised learning performance are explored quantitatively with the defined spike sequence distance. Finally, conclusions are drawn in Section IV.

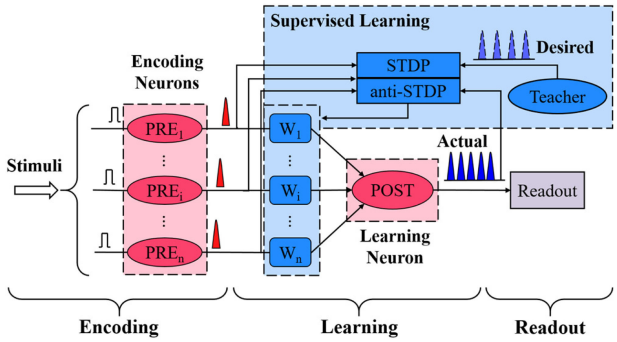

Fig. 1. Schematic diagram of a photonic SNN based on VCSEL-SAs. PRE_1-PRE_n: photonic pre-synaptic neurons; POST: photonic post-synaptic neuron; W_1-W_n: variable synapses; STDP and anti-STDP array: optical STDP and anti-STDP realized by VCSOAs; Teacher: the teacher neuron produces the desired output spike sequence to instruct the SNN; Actual: the actual output spike sequence generated by the POST.

II. Model and Method

A. Architecture of the Photonic SNN

The schematic diagram of a two-layer fully-connected photonic SNN based on VCSELs-SA for the supervised spike sequence learning is shown in Fig. 1. The VCSELs-SA are adopted to act as both the pre-synaptic neurons (PREs) and the post-synaptic neuron (POST). Here, the PREs are the encoding neurons, and the single POST is the learning neuron. The PREs are fully connected to the single POST via the variable synapses weighting modules (W_1-W_n). The number of synapses is equal to the number of encoding neurons. In this photonic SNN, the classical ReSuMe supervised learning algorithm based on the photonic STDP is adopted to train the POST to fire the desired spike sequence. Hence, the teacher neuron and the STDP/anti-STDP array are introduced to update synaptic weights. Note that, in this network, the weighting stage and the STDP stage are separated. As shown in Fig. 1, the weighting stage is accomplished by the modules W_1-W_n. In a possible experiment, a programmable variable attenuator array can be utilized to implement the weighting according to the weight update amount calculated from the STDP/anti-STDP module.

In the encoding part, the external input pulses (stimuli) are injected into the PREs to implement the spatio-temporal encoding. The function of the learning part is to make POST emit an actual output spike sequence which is consistent with the desired output spike sequence provided by the teacher neuron, by adjusting synaptic weights. During each learning epoch, the weight update is determined by the timing of the pre-synaptic spikes (t_i), post-synaptic spikes (t_o) and teacher spikes (t_d). Specially, the synaptic weight is strengthened (weakened) according to the STDP (anti-STDP) based on the time difference between t_i and t_d (t_i and t_o). Therefore, the task of spike sequence learning can be fulfilled in this architecture.

B. Photonic Neurons Based on VCSELs-SA

All spiking neurons used in the photonic SNN model are implemented by the excitable VCSEL-SA neurons which behave a similar behavior to LIF neurons. The rate equations of a

VCSEL-SA are written as follows [24], [34], [48]:

$$\dot{S_{i,o}} = \Gamma_a g_a(n_a - n_{0a})S_{i,o} + \Gamma_s g_s(n_s - n_{0s})S_{i,o} - S_{i,o}/\tau_{ph} + \beta B_r n_a^2 \quad (1)$$

$$\dot{n_a} = -\Gamma_a g_a (n_a - n_{0a}) (S - \Phi_{pre,i} - \Phi_{post,o}) - n_a/\tau_a + I_a/(eV_a) \quad (2)$$

$$\dot{n_s} = -\Gamma_s g_s(n_s - n_{0s})S_{i,o} - n_s/\tau_s + I_s/eV_s \quad (3)$$

Where the subscript $i\,(i = 1, \ldots, n)$ denotes the serial number of the PREs, and the subscript o denotes the POST. The subscripts a and s stand for the gain and absorber regions, respectively. $S_{i,o}(t)$ represent the photon density in the cavity of the PREs and POST. n_a (n_s) is the carrier density in the gain (absorber) region.

The term $\Phi_{pre,i} = k_{ei}\tau_{ph}\lambda_i P_{ei}(\tau_i, \Delta\tau)/(hcV_a)$ in Eq. (2) denotes the external input pulse (stimulus), in which k_{ei}, τ_i and $\Delta\tau$ are the strength, the central timing and the temporal duration of the pulse, respectively. Besides, we define $\Delta\tau_i = \tau_i - \tau_{i-1}$ as the time interval between two consecutive input pulses. Here, we consider $P_{ei} = 1\mathrm{mW}$. And the term $\Phi_{post,o} = \sum_{i=1}^{n} \omega_i\lambda_i\tau_{ph}P_i(t - T)/(hcV_a)$ in Eq. (2) represents the input of the POST, which is exactly the weighted sum of all the pre-synaptic spikes with transmission delay $T = 1$ ns. ω_i is the connection weight between the *i*-th PRE and the POST in the proposed SNN that can be tuned according to the supervised training method. The output power of PREs and POST are $P_{i,o}(t) \approx \eta_c\Gamma_a S_{i,o}(t)V_a hc/(\tau_{ph}\lambda_{i,o})$.

The remaining parameters are the same for all neurons, which are presented in Table I. With these parameters, the rate equations are numerically solved by using the fourth-order Runge-Kutta method.

In the proposed photonic SNN, the PREs as encoding neurons convert external stimuli into spikes by using the temporal coding, in which precise timings of spikes are taken into account for conveying information. The encoding outputs of different PREs that are subjected to rectangle pulses stimuli with different strengths (k_{ei}) and central timings (τ_i) are depicted in Fig. 2(a). It can be seen that with the increase of k_{ei}, the number of output spikes increases, while the time interval between the beginning of input pulse and the first output spike decreases. Meanwhile, as shown in Fig. 2(b), the POST as the learning neuron integrates the pre-synaptic spikes (Fig. 2(b1)) and emits a spike (Fig. 2(b3)) once its carrier density n_a reaches the threshold (Fig. 2(b2)). Obviously, these excitability dynamics of photonic neurons based on the VCSELs-SA are similar to those of biological neurons.

C. Supervised Learning Algorithm by Incorporating the Photonic STDP Based on VCSOAs: ReSuMe

The ReSuMe algorithm is derived from the Widrow-Hoff rule and employs well-recognized physiological phenomena [52]. It is based on the correlation of spike timing and aims to make the POST of the SNN emit spike sequence approximating the desired spike sequence through learning. It does not need to directly pair the actual and desired output spikes, but adjusts synaptic weights at the actual and desired output spikes respectively. Thus the desired and actual output spikes are independent of each other. To be specific, synaptic potentiation depends on the correlation between the pre-synaptic and actual firing times, while synaptic depression is based on the correlation between the pre-synaptic and desired firing times.

According to the ReSuMe learning algorithm, the total weight update amount of *i*-th synapse is:

$$\Delta\omega_i = (n_d - n_o) + \sum_{t_d}\sum_{t_i \le t_d} \Delta\omega_{STDP}(t_d - t_i) + \sum_{t_o}\sum_{t_i \le t_o} \Delta\omega_{aSTDP}(t_o - t_i) \quad (4)$$

TABLE I
VCSEL-SA EXCITABLE LASER PARAMETERS [34], [48]

Param.	Description	Value
λ_i	Lasing wavelength	850nm
β	Spontaneous emission coupling factor	1×10^{-4}
η_c	Output power coupling coefficient	0.4
B_r	Bimolecular recombination term	$10\times10^{-6}\,\mathrm{m^3s^{-1}}$
τ_{ph}	Photon lifetime	4.8ps
V_a	Gain region cavity volume	$2.4\times10^{-18}\,\mathrm{m^3}$
V_s	Absorber region cavity volume	$2.4\times10^{-18}\,\mathrm{m^3}$
Γ_a	Gain region confinement factor	0.06
Γ_s	Absorber region confinement factor	0.05
τ_a	Gain region carrier lifetime	1ns
τ_s	Absorber region carrier lifetime	100ps
g_a	Gain region differential gain/loss	$2.9\times10^{-12}\,\mathrm{m^3s^{-1}}$
g_s	Absorber region differential gain/loss	$14.5\times10^{-12}\,\mathrm{m^3s^{-1}}$
n_{0a}	Gain region transparency carrier density	$1.1\times10^{24}\,\mathrm{m^{-3}}$
n_{0s}	Absorber region transparency carrier density	$0.89\times10^{24}\,\mathrm{m^{-3}}$
I_a	Bias current in the gain region	2mA
I_s	Bias current in the absorber region	0mA

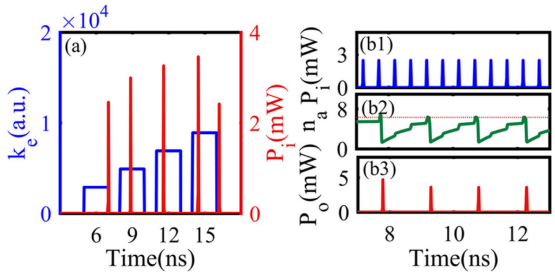

Fig. 2. (a) The temporal coding of PREs for $k_{e1} = 2.9 \times 10^3$, $\tau_1 = 6$ ns, $k_{e2} = 4.9 \times 10^3$, $\tau_2 = 9$ ns, $k_{e3} = 6.9 \times 10^3$, $\tau_3 = 12$ ns, $k_{e4} = 8.9 \times 10^3$, $\tau_4 = 15$ ns, with $\Delta\tau = 2$ ns. (b) The response process of the POST with $k_{e1} = 2.9 \times 10^3$, $\tau_1 = 2$ ns, $\Delta\tau = 2$ ns, $\Delta\tau_i = 0.5$ ns, $\omega_i = 0.1$. (b1) pre-synaptic spikes, (b2) carrier density in the POST, (b3) post-synaptic spike outputs.

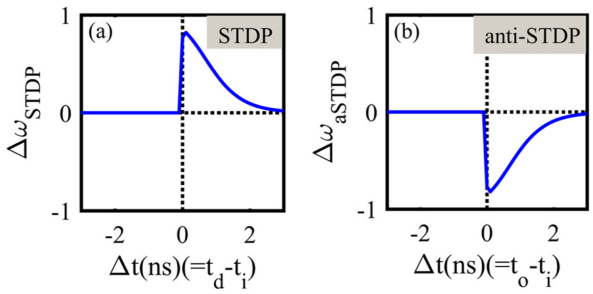

Fig. 3. (a) Photonic STDP learning window, (b) anti-STDP learning window.

Where n_d and n_o are the spikes number of the desired and the actual output spike sequences. The first term of Eq. (4) which is non-Hebbian term aims to adjust the average strength of the input synapses, such that the number of the actual output spike sequence approaches that of the desired output spike sequence. The last two terms are Hebbian terms which are mainly responsible to ensure the precise timing of spikes. The second (third) term denotes the synaptic potentiation (depression). $t_i \leq t_d$ and $t_i \leq t_o$ in Hebbian terms represent that this rule only modifies inputs that contribute to the neuron state before the desired or actual output firing time, but does not consider those inputs that fire afterward which have no contribution to the current states. In addition, the synaptic weights are not adjusted if the neuron fires at exactly the desired times.

It has been shown that, the photonic STDP implemented by a VCOSA is similar to the STDP response obtained from biological experiments [47]. The $\Delta\omega_{STDP}(t_d - t_i)$ and $\Delta\omega_{aSTDP}(t_o - t_i)$ in Eq. (4) are photonic STDP and anti-STDP learning rules, which can be calculated by [45], [47]:

$$\Delta\omega_{STDP}\left(t_d - t_i\right) = \begin{cases} \Delta\omega_o\left(\Delta t\right), & if\ t_d - t_i > 0 \\ 0, & if\ t_d - t_i \leq 0 \end{cases} \tag{5}$$

$$\Delta\omega_{aSTDP}\left(t_o - t_i\right) = \begin{cases} -\Delta\omega_o\left(\Delta t\right), & if\ t_o - t_i > 0 \\ 0, & if\ t_o - t_i \leq 0 \end{cases} \tag{6}$$

The theoretical model of VCSOAs and photonic STDP circuit are identical to those presented in our previous work [47], and are not given here again. The calculation of $\Delta\omega_0(\Delta t)$ is similar to Eq. (7) in the Ref. [47]. Here, the STDP and anti-STDP curves are calculated in advance with a single VCSOA. Then, these curves are stored and are used to update the synaptic weight through an ex-situ learning approach. Besides, it is important to ensure that the spikes from the different neurons (from the teacher, PREs, and POST) arrive within the same temporal window to the STDP/anti-STDP stage. Hence, in a possible experiment, an additional time-management module with precise variable optical delay lines is suggested to compensate for the transmission delays. Both the photonic STDP and anti-STDP learning curves, as depicted in Fig. 3, are applied in the ReSuMe algorithm. It can be seen that, the synaptic weight is potentiated if a desired output spike is observed, and is depressed once the POST fires.

During the learning phase, the modification of synaptic weight from learning epoch x to $x+1$ is computed as follows:

$$\omega_i\left(x+1\right) = \omega_i\left(x\right) + \omega_f \times \Delta\omega_i \tag{7}$$

Where $\omega_i(x)$ and $\omega_i(x+1)$ are the weights of synapse i at x-th and $(x+1)$-th learning epochs, respectively. The initial weight of synapse i is $\omega_i(0)$. ω_f stands for the learning rate, and is 0.004 in this paper, unless otherwise stated.

D. Measure of Learning Performance: Spike Sequence Distance

In the spike sequence learning, the similarity between the actual and the desired output spike sequence is used to evaluate the learning performance. The dissimilarity of a pair of spike sequences expresses at two aspects: one is the difference between the numbers of spikes from two spike sequences, and the other one is the firing time difference between the corresponding individual spikes in two spike sequences. To quantitatively estimate the learning performance of the proposed SNN, we define a spike sequence distance (*SSD*) measure by modifying the Victor & Purpura (VP) distance [53], which can be expressed as:

$$SSD = 2|_{n_o \neq n_d} + 1|_{n_o = n_d, |t_o - t_d| \geq r} + \sum_{\substack{n_o = n_d \\ |t_o - t_d| < r}} \left(|(t_o - t_d)|\,/ n_o r\right) \tag{8}$$

Where r is a precision parameter, and is a real positive value. It is suggested that the value of r is less than a half of the minimal inter-spike interval in the desired output spike sequence [54]. So we set $r = 0.2$ ns in the following simulation.

In Eq. (8), the numbers of spikes in the actual and desired output spike sequences are firstly compared. If they are not equal ($n_o \neq n_d$), which illustrates the occurrence of additional or missing spikes in the actual output spike sequence, we directly consider $SSD = 2$, as denoted in the first term. When $n_o = n_d$, all time differences between the individual corresponding spikes in two spike sequences are further judged. If $|t_o - t_d| \geq r$, the *SSD* is set to 1, as presented in the second term, to distinguish from the case with different spike numbers. Furthermore, if $|t_o - t_d| < r$, the last term is computed, which represents that the actual output spike sequence approximates the desired output spike sequence with the precision r. The range of the third term is $[0, 1)$.

Therefore, $SSD < 1$ reflects a greatly similarity between two spike sequences, and *SSD* is equal to 0 for two identical spike sequences. Consequently, the *SSD* closing to 0 represents the excellent learning performance. Note, this measure *SSD* is not involved in the ReSuMe learning rule, but is only used for measuring and analyzing the performance of the learning rule.

III. Result and Discussion

In this section, the learning process of the spike sequence is implemented and analyzed firstly. The learning performance is evaluated quantitatively with the defined spike sequence distance. Then, the effects of the initial weights and the number of

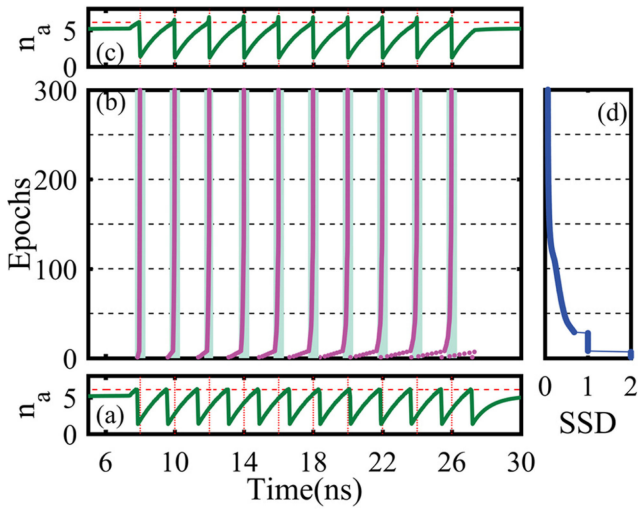

Fig. 4. Illustration of the spike sequence learning of a typical run. (a) The dynamics of POST's carrier density at the first learning epoch, (b) the learning process during the consecutive 300 learning epochs, (c) the dynamics of POST's carrier density at the last learning epochs, (d) the measure *SSD* as a function of the learning epoch. The red horizontal lines and vertical lines in (a) and (c) denote the threshold of carrier density and the desired output spike timings, respectively. The light blue bars and purple dots in (b) indicate the target spikes and actual output spikes, respectively.

PREs on the learning performance are quantified to optimize the learning algorithm.

A. Learning Process of Spike Sequences

Here, extensive simulations are carried out to illustrate the learning process of spike sequences based on our proposed photonic SNN. In all simulations, 200 PREs are fully connected to a single POST. We consider the initial weights of all 200 synapses are $\omega_i(0) = 0.02\,(i = 1, 2, \ldots, 200)$. All input pulses are set as $k_{ei} = 2.9 \times 10^3$, $\Delta\tau = 2$ ns to ensure that each PRE fires a single spike. For convenience, the center timings (τ_i) of input pulses of PREs are chronologically sorted, which determine the input spike pattern in the photonic SNN. Here, we set $\tau_1 = 5.3$ ns and $\Delta\tau_i = 0.1$ ns. The widths of the STDP and anti-STDP time windows are set as 4 ns.

Fig. 4(b) illustrates the learning process during the consecutive 300 learning epochs, which includes the desired output spike sequence denoted by light blue bars and the actual output spikes after each learning epoch denoted by purple dots. Correspondingly, the measure *SSD* as a function of the learning epoch is shown in Fig. 4(d), which reflects the learning performance after each learning epoch. In this simulation, the desired spike sequence contains ten target spikes, i.e., $t_d =$ [8 ns, 10 ns, 12 ns, 14 ns, 16 ns, 18 ns, 20 ns, 22 ns, 24 ns, 26 ns]. At the beginning of the learning, the actual output spike sequence fired at any arbitrary time is quite different from the desired output spike sequence, thus $SSD = 2$. During the learning process, the POST gradually learns to produce spikes at the desired times, and the *SSD* gradually decreases. Obviously, from the 8-th learning epoch, the number of spikes fired by the POST is the same as the number of target spikes, i.e., $SSD \leq 1$. At about 140-th epoch, the firing times of the actual output spikes almost match those in the desired spike sequence, and the corresponding *SSD* approximates to 0. As the learning process is repeated, the evolution of *SSD* along the learning shows that the learning process is convergent.

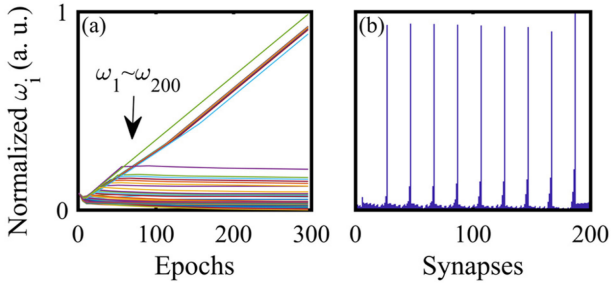

Fig. 5. (a) Weight distribution of 200 synapses during the learning process. These lines in the figure correspond to 200 synapses respectively. (b) The weights histogram of 200 synapses after training 300 epochs. The height of each bar in the histogram reflects the corresponding synaptic strength.

The dynamics of POST's carrier density n_a at the first and last learning epochs are also shown in Figs. 4(a) and 4(c). Whenever the n_a exceeds the threshold (the red horizontal line), a spike is emitted. As shown in Fig. 4(a), for the 1-st learning epoch, it is clear that the fire timings of the POST are different from the desired output spike timings which are represented by the red vertical lines. At the 300-th learning epoch, as can be seen in Fig. 4(c), the POST successfully emits spikes at ten target spike timings. These results again demonstrate that the POST successfully learns to emit at desired spike timings and reproduces the desired spike sequence.

Furthermore, the weight distribution of the 200 synapses during the learning process corresponding to Fig. 4 is depicted in Fig. 5(a). Obviously, before learning, the initial weights are identical indicating that there are no differences among the input synapses. After learning, some synaptic weights are potentiated, while others are depressed to produce the desired spike sequence. To identify which synapses are potentiated or depressed, the weights histogram of these 200 synapses after 300 learning epochs is shown in Fig. 5(b), in which each synaptic weight is reflected by the height of each bar. Obviously, the temporal causality can be revealed. Among these causal synapses, the one with a closer spiking time to the desired time has a relatively higher synaptic strength. The synapses corresponding to the pre-synaptic spikes far from the desired time have lower synaptic strength. This implies that the evolution of the POST activity is highly related to the synaptic weights.

Without loss of generality, we further investigate the ability of the photonic SNN to learn different desired spike sequences. The learning processes and corresponding *SSD* during the consecutive 300 learning epochs for three different desired spike sequences are shown in Fig. 6. The desired spike sequences corresponding to Figs. 6(a), (b) and (c) are $t_d^a =$ [8 ns, 10 ns, 12 ns, 14 ns, 16 ns, 18 ns, 20 ns, 22 ns, 24 ns], $t_d^b =$ [8 ns, 10 ns, 12 ns, 14 ns, 16 ns, 18 ns, 20 ns], and $t_d^c =$ [9 ns, 11 ns, 13 ns, 15 ns, 17 ns, 19 ns, 21 ns], respectively. It can be seen that, under different target conditions, the *SSD* can converge to a value that is close to 0 after the learning process is finished.

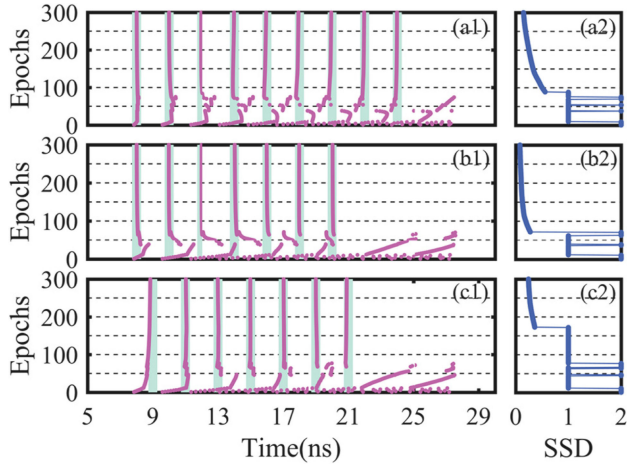

Fig. 6. The training processes of spike sequence learning (left column) and the corresponding *SSD* (right column) for (a1-a2) t_d^a = [8 ns, 10 ns, 12 ns, 14 ns, 16 ns, 18 ns, 20 ns, 22 ns, 24 ns], (b1-b2) t_d^b = [8 ns, 10 ns, 12 ns, 14 ns, 16 ns, 18 ns, 20 ns], (c1-c2) t_d^c = [9 ns, 11 ns, 13 ns, 15 ns, 17 ns, 19 ns, 21 ns].

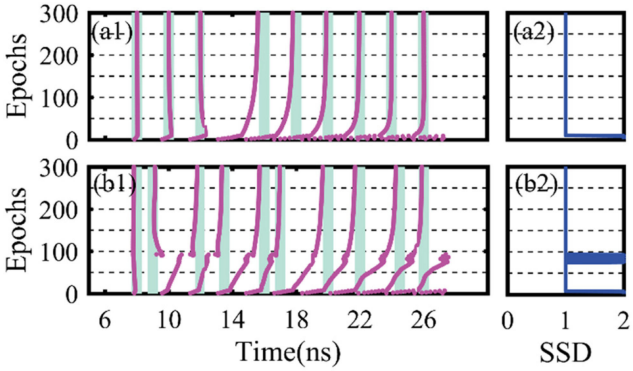

Fig. 7. The training processes of spike sequence learning (left column) and the corresponding *SSD* (right column) during the consecutive 300 learning epochs for (a1-a2) t_{d1} = [8 ns, 10 ns, 12 ns, 16 ns, 18 ns, 20 ns, 22 ns, 24 ns, 26 ns], (b1-b2) t_{d2} = [8 ns, 9 ns, 12 ns, 13.5 ns, 16 ns, 17 ns, 20 ns, 22 ns, 24.5 ns, 26 ns].

Therefore, the proposed photonic SNN can perform the spike sequence learning efficiently.

In above simulations, we analyze the response of proposed network using spike sequences with equidistant spikes, i.e., the inter-spike intervals are equal to 2ns in all cases. Here, we further consider the learning processes and corresponding *SSD* during the consecutive 300 learning epochs for other cases in Fig. 7. As shown in Fig. 7(a), gaps with missing spikes are introduced in the sequence, and the desired spike sequence is t_{d1} = [8 ns, 10 ns, 12 ns, 16 ns, 18 ns, 20 ns, 22 ns, 24 ns, 26 ns] which contains nine target spikes and lacks a target spike of 14ns. And Fig. 7(b) depicts the case that different time-separations between spikes are configured, in which the desired spike sequence is t_{d2} = [8 ns, 9 ns, 12 ns, 13.5 ns, 16 ns, 17 ns, 20 ns, 22 ns, 24.5 ns, 26 ns]. For these two cases, the learning processes during the consecutive 300 learning epochs show that the POST can emit spikes near desired spike timings. But the values of *SSD* illustrate that there is a certain deviation between the actual and desired

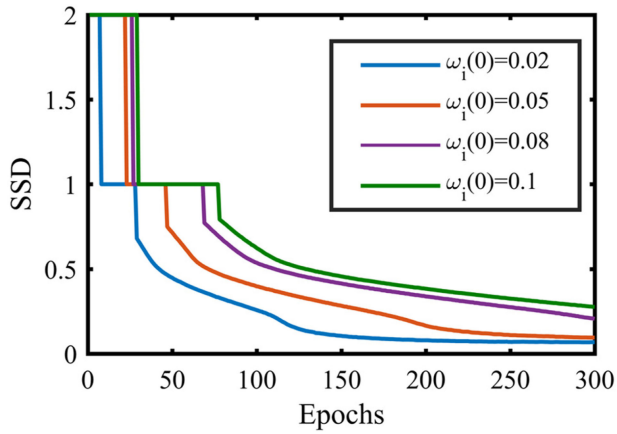

Fig. 8. The variation of *SSD* during the consecutive 300 learning epochs for $\omega_i(0) = 0.02, 0.05, 0.08, 0.1$.

output spike sequences. As the learning epoch increases to 500, the results (not shown here) are almost the same as those shown in Fig. 7. It is found that the maximum deviation between the actual and target spikes approximates 0.4ns. Compared to the case of the desired spike sequences with equidistant spikes, the deviation between the actual and desired output spikes increases in the case of sequence with non-equidistant spikes.

B. Optimization of the Learning Algorithm

Through extensive simulations, we found that the learning performance of the proposed SNN can be improved by optimizing certain parameters.

We perform similar simulations at different initial weights $\omega_i(0)$ to analyze the effect of the initial weight on the learning performance of the spike sequence. Fig. 8 shows the variation of *SSD* during the consecutive 300 learning epochs for different $\omega_i(0)$. Here, the desired spike sequence is t_d = [8 ns, 10 ns, 12 ns, 14 ns, 16 ns, 18 ns, 20 ns, 22 ns, 24 ns, 26 ns]. The results demonstrate that the learning processes are all convergent for these different $\omega_i(0)$. Meanwhile, it is found that the convergent epochs are slightly different for distinct $\omega_i(0)$. Hence, the initial weight modifies the learning process slightly.

In addition, the impact of the number of PREs on the learning performance of the network is investigated. Fig. 9 depicts the actual output spikes (purple dots) generated by the POST and the corresponding *SSD* at the 300-th and 500-th learning epochs for different number of PREs which ranges from 10 to 600 with the interval of 10. The desired spike sequence is t_d = [8 ns, 10 ns, 12 ns, 14 ns, 16 ns, 18 ns, 20 ns, 22 ns, 24 ns, 26 ns], and other simulation conditions are consistent with the above simulation. It is clear that, for a relatively few number of PREs, the learning is failed at the 300-th and 500-th learning epochs. With the gradual increase of the number of PREs (from bottom to top in Fig. 9), the spike sequence generated by the POST is gradually close to the desired output spike sequence. As the number of PREs increases further, the value of *SSD* fluctuates and is still higher than the *SSD* for 200 PREs. Hence, as can be seen in Figs. 9(a2) and (b2), the minimal *SSD* is obtained

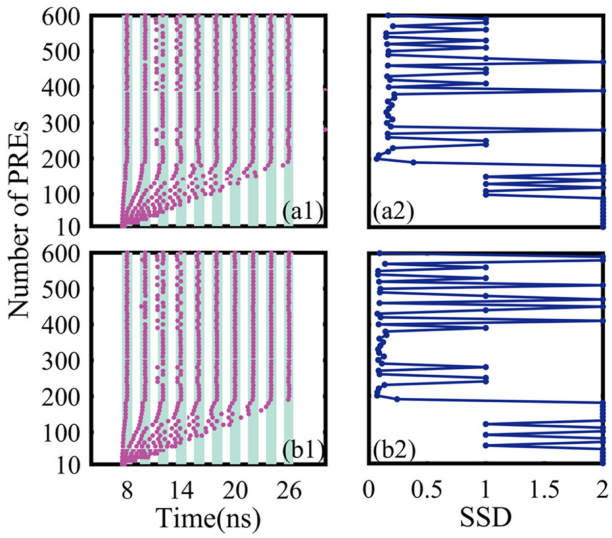

Fig. 9. The actual output spikes (purple dots) generated by the POST (left column) and corresponding *SSD* (right column) for different number of PREs which ranges from 10 to 600 with the interval of 10 (from bottom to top), (a1, a2) at the 300-th learning epoch, (b1, b2) at the 500-th learning epoch, with ten target spikes (light blue bars).

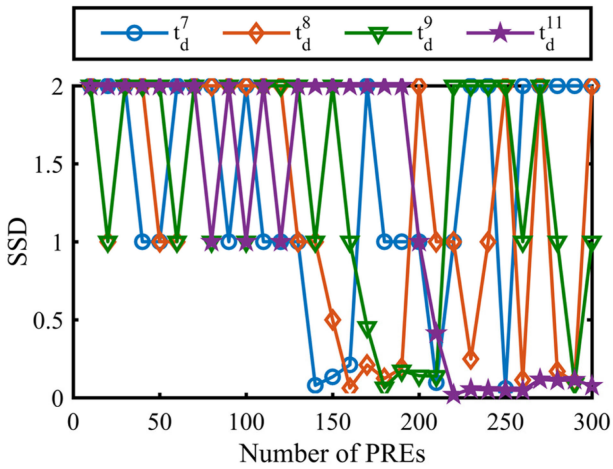

Fig. 10. The *SSD* at the 300-th learning epoch as a function of the number of PREs for the desired spike sequences with different numbers of target spikes. t_d^7 = [8 ns, 10 ns, 12 ns, 14 ns, 16 ns, 18 ns, 20 ns], t_d^8 = [8 ns, 10 ns, 12 ns, 14 ns, 16 ns, 18 ns, 20 ns, 22 ns], t_d^9 = [8 ns, 10 ns, 12 ns, 14 ns, 16 ns, 18 ns, 20 ns, 22 ns, 24 ns], t_d^{11} = [8 ns, 10 ns, 12 ns, 14 ns, 16 ns, 18 ns, 20 ns, 22 ns, 24 ns, 26 ns, 28 ns].

when the number of PREs is 200, which represents the optimal performance. Even the values of *SSD* for some cases with more than 200 PREs are also low and even similar to that for the case with 200 PREs, the less number of PREs is desired for the purpose of low power consumption. Hence, the optimal PREs number is hardly affected by the fluctuation of *SSD* with the increase of the number of PREs.

At last, to explore the relationship between the number of PREs and desired spike sequences, similar analyses are performed for desired spike sequences with different numbers of target spikes. As shown in Fig. 10, the measure *SSD* at the 300-th learning epoch is plotted as a function of the number of PREs, and different curves represent desired output sequences with different spike numbers. These desired output sequences are t_d^7 = [8 ns, 10 ns, 12 ns, 14 ns, 16 ns, 18 ns, 20 ns], t_d^8 = [8 ns, 10 ns, 12 ns, 14 ns, 16 ns, 18 ns, 20 ns, 22 ns], t_d^9 = [8 ns, 10 ns, 12 ns, 14 ns, 16 ns, 18 ns, 20 ns, 22 ns, 24 ns], and t_d^{11} = [8 ns, 10 ns, 12 ns, 14 ns, 16 ns, 18 ns, 20 ns, 22 ns, 24 ns, 26 ns, 28 ns], respectively. It can be seen that the optimal PREs numbers are 140, 160, 180 and 220 for desired output sequences with 7, 8, 9 and 11 spikes, respectively. Note, for the case of t_d^7, the values of *SSD* for both cases of 140 PREs and 250 PREs are low. Considering that fewer VCSEL-SA neurons are beneficial to the actual construction of the network with lower power consumption, thus we adopt 140 PREs as the optimal number for the case of t_d^7. Interestingly, it is found that, 20 PREs are required for each additional target spike in the desired spike sequence. That is to say, 20 PREs are responsible for the output of a spike under the specific input pattern in this photonic SNN.

IV. Conclusion

In summary, we proposed a fully-connected photonic SNN composed of VCSEL-SAs for supervised spike sequence learning. The photonic STDP is incorporated into a classical ReSuMe algorithm. Moreover, a spike sequence distance measure is proposed to evaluate quantitatively the learning performance. The numerical results show that, the supervised learning algorithm can be optimized thanks to the unified model of the photonic SNN. It is found that, the supervised training enables learning different target spikes with different spike numbers. Besides, an optimal number of pre-synaptic neurons exists for a given target spike number. These results provide guidelines for constructing a functional photonic SNN based on VCSELs-SA for spike sequence learning.

References

[1] F. Javed *et al.*, "Brain and high metabolic rate organ mass: Contributions to resting energy expenditure beyond fat-free mass," *Amer. J. Clin. Nutrition*, vol. 91, no. 4, pp. 907–912, Apr. 2010.
[2] A. M. Turing, "Mind," *Mind*, vol. 59, no. 236, pp. 433–460, Oct. 1950.
[3] I. A. Basheer and M. Hajmeer, "Artificial neural networks: Fundamentals, computing, design, and application," *J. Microbiological Methods*, vol. 43, no. 1, pp. 3–31, Dec. 2000.
[4] C. A. Runyan, E. Piasini, S. Panzeri, and C. D. Harvey, "Distinct timescales of population coding across cortex," *Nature*, vol. 548, pp. 92–96, Jul. 2017.
[5] S. M. Bohte, "The evidence for neural information processing with precise spike-times: A survey," *Natural Comput.*, vol. 3, no. 2, pp. 195–206, Jun. 2004.
[6] W. Maass, "Networks of spiking neurons: The third generation of neural network models," *Neural Netw.*, vol. 10, no. 9, pp. 1659–1671, Dec. 1997.
[7] S. Ghosh-Dastidar and H. Adeli, "Spiking neural networks," *Int. J. Neural Syst.*, vol. 19, no. 04, pp. 295–308, 2009.
[8] K. Roy, J. Akhilesh, and P. Priyadarshini, "Towards spike-based machine intelligence with neuromorphic computing," *Nature*, vol. 575, pp. 607–617, Nov. 2019.
[9] C. Mead, "Neuromorphic electronic systems," *Proc. IEEE*, vol. 78, no. 10, pp. 1629–1636, Oct. 1990.
[10] D. Tank and J. J. Hopfield, "Simple 'neural' optimization networks: An A/D converter, signal decision circuit, and a linear programming circuit," *IEEE Trans. Circuits Syst.*, vol. 33, no. 5, pp. 533–541, May 1986.

[11] I. Sourikopoulos *et al.*, "A 4-fJ/spike artificial neuron in 65 nm CMOS technology," *Front. Neuroscience*, vol. 11, Mar. 2017, Art. no. 123.

[12] J. Shi, S. D. Ha, Y. Zhou, F. Schoofs, and S. Ramanathan, "A correlated nickelate synaptic transistor," *Nature Commun.*, vol. 4, Oct. 2013, Art. no. 2676.

[13] W. Xu, S. Y. Min, H. Hwang, and T. W. Lee, "Organic core-sheath nanowire artificial synapses with femtojoule energy consumption," *Sci. Advances*, vol. 2, no. 6, Jun. 2016, Art. no. e1501326.

[14] J. Zhu *et al.*, "Ion gated synaptic transistors based on 2D van der Waals crystals with tunable diffusive dynamics," *Adv. Mater.*, vol. 30, no. 21, Apr. 2018, Art. no. 1800195.

[15] M. Prezioso *et al.*, "Training and operation of an integrated neuromorphic network based on metal-oxide memristors," *Nature*, vol. 521, pp. 61–64, May 2015.

[16] S. Park *et al.*, "Electronic system with memristive synapses for pattern recognition," *Sci. Rep.*, vol. 5, May 2015, Art. no. 10123.

[17] I. Boybat *et al.*, "Neuromorphic computing with multi-memristive synapses," *Nature Commun.*, vol. 9, no. 1, 2018, Art. no. 2514.

[18] S. G. Hu *et al.*, "An improved memristor model connecting plastic synapse and nonlinear spiking neuron," *J. Phys. D: Appl. Phys.*, vol. 52, no. 27, May 2019, Art. no. 275402.

[19] A. F. Benner, M. Ignatowski, J. A. Kash, D. M. Kuchta, and M. B. Ritter, "Exploitation of optical interconnects in future server architectures," *IBM J. Res. Devlop.*, vol. 49, no. 4.5, pp. 755–775. Jul. 2005.

[20] A. Hurtado, I. D. Henning, and M. J. Adams, "Optical neuron using polarization switching in a 1550 nm-VCSEL," *Opt. Express*, vol. 18, no. 24, pp. 25170–25176, Nov. 2010.

[21] W. Coomans, L. Gelens, S. Beri, J. Danckaert, and G. Van der Sande, "Solitary and coupled semiconductor ring lasers as optical spiking neurons," *Phys. Rev. E*, vol. 84, no. 3, Sep. 2011, Art. no. 036209.

[22] A. Hurtado, K. Schires, I. D. Henning, and M. J. Adams, "Investigation of vertical cavity surface emitting laser dynamics for neuromorphic photonic systems," *Appl. Phys. Lett.*, vol. 100, no. 10, Mar. 2012, Art. no. 103703.

[23] T. V. Vaerenbergh *et al.*, "Cascadable excitability in microrings," *Opt. Express*, vol. 20, no. 18, pp. 20292–20308, Aug. 2012.

[24] M. A. Nahmias, B. J. Shastri, A. N. Tait, and P. R. Prucnal, "A leaky integrate-and-fire laser neuron for ultrafast cognitive computing," *IEEE J. Sel. Topics Quantum Electron.*, vol. 19, no. 5, Sep./Oct. 2013, Art. no. 1800212.

[25] F. Selmi *et al.*, "Relative refractory period in an excitable semiconductor laser," *Phys. Rev. Lett.*, vol. 112, no. 18, May 2014, Art. no. 183902.

[26] B. J. Shastri *et al.*, "Spike processing with a graphene excitable laser," *Sci. Rep.*, vol. 6, Jan. 2016, Art. no. 19126.

[27] B. Romeira, R. Avo, J. M. L. Figueiredo, S. Barland, and J. Javaloyes, "Regenerative memory in time-delayed neuromorphic photonic resonators," *Sci. Rep.*, vol. 6, Jan. 2016, Art. no. 19510.

[28] P. R. Prucnal, B. J. Shastri, T. F. De Lima, M. A. Nahmias, and A. N. Tait, "Recent progress in semiconductor excitable lasers for photonic spike processing," *Advances Opt. Photon.*, vol. 8, no. 2, pp. 228–299, Jun. 2016.

[29] S. Y. Xiang *et al.*, "Cascadable neuron-like spiking dynamics in coupled VCSELs subject to orthogonally polarized optical pulse injection," *IEEE J. Sel. Topics Quantum Electron.*, vol. 23, no. 6, Nov./Dec. 2017, Art. no. 1700207.

[30] T. Deng, J. Robertson, and A. Hurtado, "Controlled propagation of spiking dynamics in vertical-cavity surface-emitting lasers: Towards neuromorphic photonic networks," *IEEE J. Sel. Topics Quantum Electron.*, vol. 23, no. 6, Nov./Dec. 2017, Art. no. 1800408.

[31] J. Robertson, T. Deng, J. Javaloyes, and A. Hurtado, "Controlled inhibition of spiking dynamics in VCSELs for neuromorphic photonics: Theory and experiments," *Opt. Lett.*, vol. 42, no. 8, pp. 1560–1563, Apr. 2017.

[32] J. Robertson, E. Wade, Y. Kopp, J. Bueno, and A. Hurtado, "Toward neuromorphic photonic networks of ultrafast spiking laser neurons," *IEEE J. Sel. Topics Quantum Electron.*, vol. 26, no. 1, Jan./Feb. 2020, Art. no. 7700715.

[33] S. Y. Xiang, Y. H. Zhang, X. X. Guo, A. J. Wen, and Y. Hao, "Photonic generation of neuron-like dynamics using VCSELs subject to double polarized optical injection," *J. Lightw. Technol.*, vol. 36, no. 19, pp. 4227–4234, Oct. 2018.

[34] Y. H. Zhang *et al.*, "Spike encoding and storage properties in mutually coupled vertical-cavity surface-emitting lasers subject to optical pulse injection," *Appl. Opt.*, vol. 57, no. 7, pp. 1731–1737, Mar. 2018.

[35] Y. H. Zhang, S. Y. Xiang, X. X. Guo, A. J. Wen, and Y. Hao, "Polarization-resolved and polarization-multiplexed spike encoding properties in photonic neuron based on VCSEL-SA," *Sci. Rep.*, vol. 8, Oct. 2018, Art. no. 16095.

[36] Y. H. Zhang, S. Y. Xiang, X. X. Guo, A. J. Wen, and Y. Hao, "All-optical inhibitory dynamics in photonic neuron based on polarization mode competition in a VCSEL with an embedded saturable absorber," *Opt. Lett.*, vol. 44, no. 7, pp. 1548–1551, Mar. 2019.

[37] Z. W. Song *et al.*, "Photonic spiking neural network based on excitable VCSELs-SA for sound azimuth detection," *Opt. Express*, vol. 28, no. 2, pp. 1561–1573, Jan. 2020.

[38] S. Xiang, Z. Ren, Y. Zhang, Z. Song, and Y. Hao, "All-optical neuromorphic XOR operation with inhibitory dynamics of a single photonic spiking neuron based on VCSEL-SA," *Opt. Lett.*, vol. 45, no. 5, pp. 1104–1107, Feb. 2020.

[39] N. Jiang *et al.*, "Simultaneous bandwidth-enhanced and time delay signature-suppressed chaos generation in semiconductor laser subject to feedback from parallel coupling ring resonators," *Opt. Express*, vol. 28, no. 2, pp. 1999–2009, Jan. 2020.

[40] M. P. Fok, Y. Tian, D. Rosenbluth, and P. R. Prucnal, "Pulse lead/lag timing detection for adaptive feedback and control based on optical spike-timing-dependent plasticity," *Opt. Lett.*, vol. 38, no. 4, pp. 419–421, Feb. 2013.

[41] R. Toole and M. P. Fok, "Photonic implementation of a neuronal algorithm applicable towards angle of arrival detection and localization," *Opt. Express*, vol. 23, no. 12, pp. 16133–16141, Jun. 2015.

[42] Q. Ren, Y. Zhang, R. Wang, and J. Zhao, "Optical spike-timing-dependent plasticity with weight-dependent learning window and reward modulation," *Opt. Express*, vol. 23, no. 19, pp. 25247–25258, Sep. 2015.

[43] B. Gholipour *et al.*, "Amorphous metal-sulphide microfibers enable photonic synapses for brain-like computing," *Adv. Opt. Mater.*, vol. 3, no. 5, pp. 635–641, Jan. 2015.

[44] R. Toole *et al.*, "Photonic implementation of spike-timing-dependent plasticity and learning algorithms of biological neural systems," *J. Lightw. Technol.*, vol. 34, no. 2, pp. 470–476, Jan. 2016.

[45] Q. Li *et al.*, "Optical implementation of neural learning algorithms based on cross-gain modulation in a semiconductor optical amplifier," *Proc. SPIE*, vol. 10019 , Oct. 2016, Art. no. 100190E-1.

[46] Z. Cheng, C. Ríos, W. H. P. Pernice, C. D. Wright, and H. Bhaskaran, "On-chip photonic synapse," *Sci. Adv.*, vol. 3, no. 9, Sep. 2017, Art. no. e1700160.

[47] S. Y. Xiang *et al.*, "Numerical implementation of wavelength-dependent photonic spike timing dependent plasticity based on VCSOA," *IEEE J. Quantum Electron.*, vol. 54, no. 6, Dec. 2018, Art. no. 8100107.

[48] S. Y. Xiang *et al.*, "STDP-based unsupervised spike pattern learning in a photonic spiking neural network with VCSELs and VCSOAs," *IEEE J. Sel. Top. Quantum Electron.*, vol. 25, no. 6, Nov./Dec. 2019, Art. no. 1700109.

[49] J. F. Seurin *et al.*, "High-efficiency VCSEL arrays for illumination and sensing in consumer applications," *Proc. SPIE*, vol. 9766, Mar. 2016, Art. no. 97660D.

[50] F. Ponulak and A. Kasi´nski, "Introduction to spiking neural networks: Information processing, learning and applications," *Acta Neurobiologiae Experimentalis*, vol. 71, no. 4, pp. 409–433, Jan. 2011.

[51] H. Jörntell and C. Hansel, "Synaptic memories upside down: Bidirectional plasticity at cerebellar parallel fiber-Purkinje cell synapses," *Neuron*, vol. 52, no. 2, pp. 227–238, Oct. 2006.

[52] F. Ponulak and A. Kasiński, "Supervised learning in spiking neural networks with ReSuMe: Sequence learning, classification, and spike shifting," *Neural Comput.*, vol. 22, no. 2, pp. 467–510, Feb. 2010.

[53] J. D. Victor and K. P. Purpura, "Metric-space analysis of spike trains: theory, algorithms and application," *Netw.: Comput. Neural Syst.*, vol. 8, no. 2, pp. 127–164, 1997.

[54] F. Ponulak, "Supervised learning in spiking neural networks with ReSuMe method," Ph.D. dissertation, Dept. Elect. Eng., Poznań Univ. Technology, Poznań, Poland, 2006.

Ziwei Song was born in Jiaozuo, China, in 1996. She is currently working toward the M.S. degree from Xidian University, Xi'an, China. Her research interests include the vertical cavity surface-emitting lasers, neuromorphic photonic systems, photonic spiking neural network.

Shuiying Xiang was born in Ji'an, China, in 1986. She received the Ph.D. degree from Southwest Jiaotong University, Chengdu, China, in 2013.

She is currently a Professor with the State Key Laboratory of Integrated Service Networks, Xidian University, Xi'an, China. She is the author or coauthor of more than 80 research papers. Her research interests include neuromorphic photonic systems, brain-inspired information processing, spiking neural network, vertical cavity surface-emitting lasers, and semiconductor lasers dynamics.

Zhenxing Ren was born in Baoji, China, in 1996. He is currently working toward the master's degree with Xidian University, Xi'an, China. His research interests include machine learning, spiking neural network.

Genquan Han was born in Hengshui, China, in 1979. He received the B.Eng. degree from Tsinghua University, Beijing, China, and the Ph.D. degree from the Institute of Semiconductors, Chinese Academy of Sciences, Beijing, in 2008.

He is currently a Professor with Xidian University, Xi'an, China. His current research interests include advanced CMOS, photonics devices, and wide bandgap materials and devices.

Yue Hao was born in Chongqing, China, in 1958. He received the Ph.D. degree from Xi'an Jiao tong University, Xi'an, in 1991.

He is currently a Professor with the State Key Discipline Laboratory of Wide Bandgap Semiconductor Technology, School of Microelectronics, Xidian University, Xi'an. His research interests include wide forbidden band semiconductor materials and devices.